Uncover: MT transect across the Western Gawler Craton and Eucla Basin

Thesis submitted in accordance with the requirements of the University of Adelaide for an Honours Degree in Geophysics.

Brad Cox

November 2015

THE UNIVERSITY of ADELAIDE

ABSTRACT

The Eucla Basin in Southern Australia is a Tertiary Basin, which covers Proterozoic crust between the Yilgarn Craton in Western Australia and the Gawler Craton in South Australia. However, very little is known of the crustal framework of this major orogenic belt, and as a result, the geological evolution of the area is poorly understood. In 2014, a deep reflection seismic and magnetotelluric (MT) transect was undertaken to provide new constraints on the survey area. The MT profile was 830 km long, with 167 stations separated 5 km apart. Broadband MT responses were obtained at all sites in the bandwidth of 200 – 0.0005 Hz (0.005-2,000 s) which records data from the top 100 m, up to 100 km in depth.

The MT responses showed different characteristcs along the line. In the western 500 km of the profile, the responses were approximately 1D and were more sensitive to the presence of thick sedimentary sequences with high porosity. For much of the Eucla Basin, the sedimentary thickness was about 500 m, but in places reached depths of around 2 km. Two dimensional inversion revealed a generally very electrically resistive upper crust of > 1,000 Ohm.m, but more conductive lower crust of < 100 Ohm.m. However, the lower crustal conductive regions were not continuous, indicating that there are significant crustal domains with different thermal and fluid evolutions.

In the eastern 300 km of the survey, the Eucla basin sediments thin and the profile crosses major shear zones and the western extent of the Gawler Craton. The MT responses here are much more three dimensional and the crust appears to be much more electrically heterogeneous.

KEYWORDS

Magnetotellurics, Eucla Basin, Gawler Craton, Crust, Upper Mantle

TABLE OF CONTENTS

LIST OF FIGURES

INTRODUCTION

The Yilgarn and Gawler cratons are both regions of Precambrian basement rock and make up a significant block of Australia's ancient continental crust (Betts et al., 2002). Both cratons are partially covered by sediment but outcrop in some areas and can be studied to a certain extent. The basement rock between these two regions however, has been far less studied, largely due to concealment by the Eucla Basin (Clarke et al., 2003). The Albany-Fraser Province, overprinting the south-eastern extent of the Yilgarn Craton and the Madura province to the east, are both partially concealed, while the Coompana Province is entirely concealed beneath the Eucla Basin (Aitken et al., 2015). The basement rocks are of interest in these regions, partly because a large percentage of mineral systems lie on the margin of cratons (Groves et al., 2007). The eastern, unconcealed extent of the Gawler Craton has world class ore bodies while the western margin remains comparitively unexplored. This leads to the possibility of mineral exploration here in the future, if early study brings positive results. The basement beneath the Eucla sediments is also of interest, mostly due to the significantly low amount of geological information currently available here. The crustal and mantle properties of these regions therefore remain relatively unknown and are of significant interest due to prospectivity and a present general lack of knowledge.

A magnetotelluric (MT) survey was performed in 2014 by Geoscience Australia, with the main intention of identifying the broad-scale crust and upper mantle structure of a profile spanning 830 km across the Eucla Basin and the Gawler Craton. The transect crosses a large intracratonic area of the Australian crust which is relatively unexplored and poorly understood. This survey is part of a bigger program conducted by Geoscience Australia named AusLAMP (the Australian Lithospheric Architecture

Magnetotelluric Project). This program began in Victoria in November 2013 and is aimed at eventually studying the lithospheric and asthenospheric properties of Australia as a whole.

The Eucla Basin is an expanse of mostly sedimentary carbonate rocks from the Cenozoic Era, covering an area both onshore and offshore. Little work has been done in this area resulting in a lack of geophysical information, largely due to the extensive size and aridity of the basin (Clarke et al., 2003). A set of Eocene sequences within the basin is believed to be indicative of major sea level changes, showing alternating periods of marine and non-marine environments throughout this time (Hou et al., 2006). The Eucla Basin may be host to a variety of crustal sequences which when studied may provide an insight into the geological evolution of the area. In addition to this, regional study may identify these geological structures as potentially holding ore minerals. This study aims to reduce this lack of knowledge and simultaneously investigate and analyse any areas of interest in this region.

This paper focusses on MT data which have been collected on an 830 km line along the Trans-Australian railway which transects the basin. This survey recorded information from 167 stations at a site spacing of 5 km, coincident with a deep seismic reflection line of the same length. Geophysical techniques are be used to study these two data forms and correlate them to one another for a more precise interpretation of the area. Gravity and magnetic surveys unrelated to this MT line have been performed over the basin in past projects. This data can be integrated with the MT results to provide a further understanding of the crustal and upper mantle geodynamics and framework. Lastly this study determines the possibility of the future prospectivity in the area. The seismic and MT data can be used to study geological structures particularly in the sub

Eucla Basin, assessing them for economic potential. Figure 1 shows gravity and magnetic results overlain by the MT survey line.

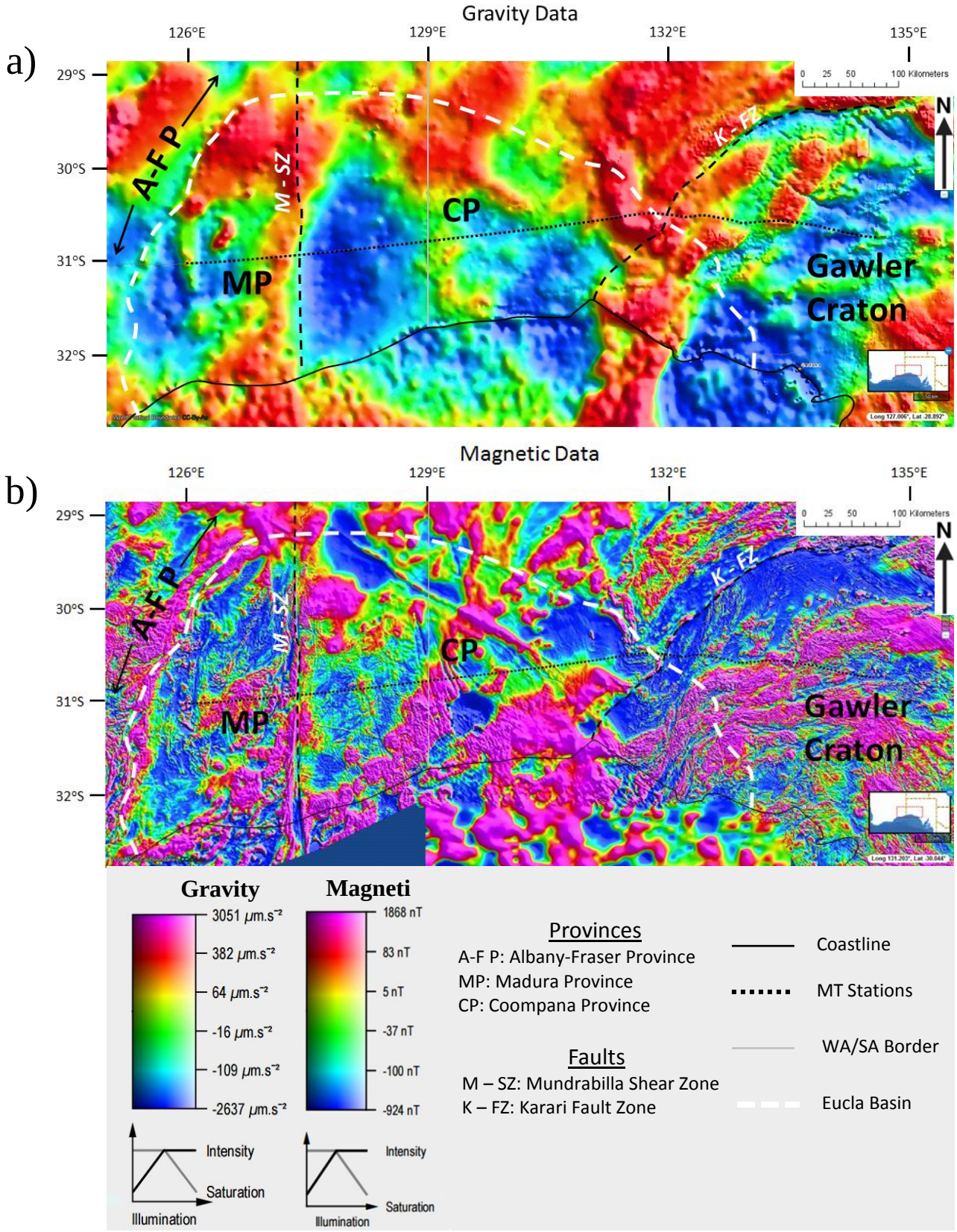

Figure 1 (a&b): The location of the 2014 MT survey plotted on gravity (a) and magnetic (b) data. Image modified from Geoscience Australia

GEOLOGICAL SETTING AND BACKGROUND

The Eucla Basin is much younger in age than the regions surrounding it. These neighbouring areas can be broken up and identified on a large scale, with the Yilgarn Craton to the west, the Gawler Craton directly to the east and the Musgrave Province to the north of the basin. These three regions are comprised of Precambrian lithologies and make up the basement rock in these areas. The Eucla Basin, lying between these cratonic blocks, contains Cretaceous sediments and therefore is expected to exhibit differing geological and geophysical properties to any nearby areas.

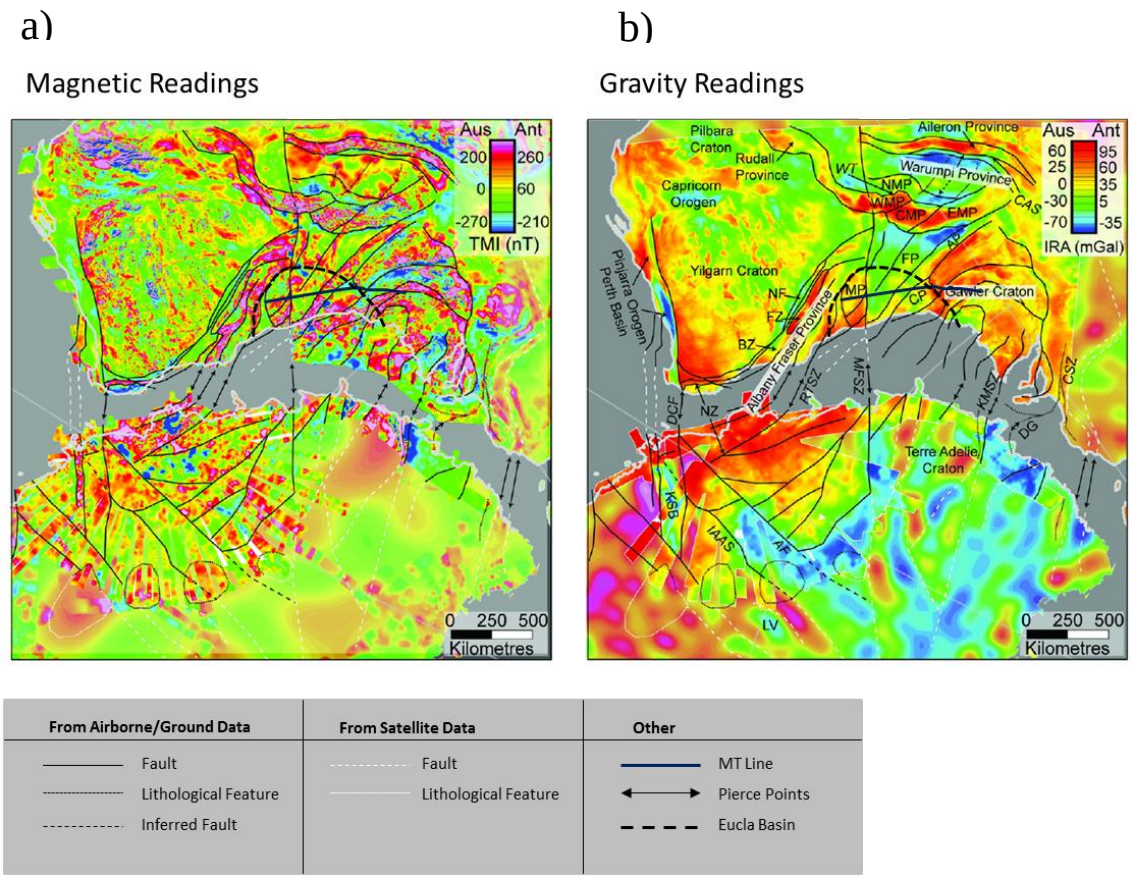

Figure 2 (a&b): Magnetic (a) and Gravity (b) Maps of Australia and Antarctica overlain by the location of the MT survey. Major faults (labelled in italics) and lithological features are also identified and inferred. Image modified from Aitken et al.

Looking at these regions closer reveals a number of provinces both near the Eucla Basin and forming part of the basin itself. To the east of the Eucla Basin is the Albany-Fraser Province, which is a region recording a number of tectonic events from the late Paleopreterozoic and Mesoproterozoic (Aitken et al., 2015). This province fits in between the Yilgarn Craton and the Madura Province and contains a number of fault zones running roughly north east – south west between the two. Spaggiari et al. (2015) and Betts et al. (2002) have identified that the Albany-Fraser province provides a well-preserved example of an Archean craton margin with noticeable signs of Proterozoic alterations. These Proterozoic processes are believed to have been active around the same time as early basin formation, which resulted from extensional forces throughout the area.

To the east of the Albany-Fraser Orogeny is the Madura Province which is overlain by the western Eucla Basin and is truncated at the Mundrabilla Shear Zone. This region was most likely formed as an oceanic arc and consists of Mid-Mesoproterozoic lithologies (Aitken et al., 2015).

Continuing east across the Mundrabilla Shear Zone, the Coompana Province appears, spanning the remainder of the Eucla Basin to the Gawler Craton (Spaggiari et al., 2015). Crossing the Mundrabilla Fault Zone from west to east is accompanied by a 200 Ma age increase into the western Coompana Province. Very limited information is known about this area due to the region being entirely concealed by sediment (Aitken et al., 2015). Major zones of faulting separate this region from the western Gawler Craton and the Musgrave Province to the north.

Finally, the Gawler Craton is the eastern-most structure in this sequence, made up of predominantly early Paleoproterozoic lithologies. This region contains numerous highly

prospective areas and makes up the bulk of the South Australian basement rock.
As the Eucla Basin overlies much of the study area, it is likely to have a significant effect on the results from any geophysical techniques used in the study. Therefore while the MT and seismics will look at responses from the crust and upper mantle, the basin sediments will be briefly acknowledged.

Geological History of the Eucla Basin

The Eucla Basin contains an extensive stratigraphic and tectonic history of southern Australia throughout the Cenozoic (Mcgowran 1989). One limitation in the study of the Eucla Basin is the sheer size of the area, which has resulted in differing geological processes acting on various areas of the basin simultaneously. The basin therefore not only has varying properties with respect to deposition time, but also with respect to location. Overall, the area is characterised by alternating marine and non-marine conditions (Mcgowran 1989) which suggest changing sea levels, coupled with significant tilting of the Australian continent.
One factor which appears to be consistent across the entire basin is water temperature. Seismic interpretation of the western region of the offshore Eucla Basin suggests that the 700m thick package was deposited largely during a cold-water period (Li et al., 1996). An exception to these conditions was in effect during the formation of the 'Little Barrier Reef', active in the middle Miocene. The formation of this carbonate platform would be due to a short-lived warm-water sedimentation period. This would likely be brought about by a strong eastward proto-Leeuwin Current bringing warmer waters from the Indian Ocean. (Feary et al., 1995).

Benbow (1990) ran a study in the Eucla Basin, focussing on a series of coastal sand dunes. The study concludes that after a marine transgression at the end of the Eocene, a series of coastal Aeolian landforms were deposited and have been preserved in the Eucla Basin. The Ooldea Range is one of these landforms which is a coastal dune 650 km long and exists 25-300 km from the present coast. Other ranges included here are the Barton and Paling ranges (Benbow, 1990). It is expected that all three were met with a high sediment load supplied by various rivers. Their preservation for 34-37 million years is likely due to vegetation cover and large periods of widespread aridity (Benbow, 1990). During the Neogene, an apparent tilt occurred across the Eucla region, with a West-side up, East-side down movement of somewhere between 100 and 200 metres. This movement may also be related to the North-down-southwest-up tilting of the Australian continent which is associated with northward plate motion (6-7cm/yr.) since around 43 Ma (Hou et al., 2008).

Geology of the Eucla Basin and Western Gawler Craton

The MT survey undertaken covers a stretch of land starting in the western Gawler Craton and heading roughly 830 kms west through the Eucla Basin.

These two areas differ in age significantly. The maximum depositional ages in the western Gawler Craton are shown by zircon dating to be between 1760 and 1700 Ma (Howard et al., 2011).

Lithologies in the Eucla Basin are much younger and include some modern day sequences covering the underlying basement rock. The sedimentary record of the Eucla basin shows four major stratigraphic layers all of Eocene age (Hou et al., 2006).

The eastern sample sites have a high level of complexity as they cover the boundary between the Eucla Basin and the Gawler Craton. This boundary is particularly complex as the very eastern extent of the Eucla Basin lies on top of the western extent of the Gawler Craton resulting in overlapping of the two provinces.

A paper written by Mclean et al. (2003) was concentrated on the shear zones and the geometry of the Hiltaba Suite granites in the western Gawler Craton. This study finds that the intrusion of these 1590-1575 Ma granites led to the formation of a large magmatic event in the Gawler Craton. From the use of gravity surveys and magnetic data the intrusions appear to be around 15-25 km in diameter and are less than 6 km deep. Major shear zones and their spatial relationship to intrusions have also been studied through gravity and magnetics (Mclean et al., 2003). The geophysical data studied in the central western Gawler Craton show complex crustal structural properties with a series of shear zones. Much of the Gawler Craton's western extent is unexposed and therefore difficult to study (Hand et al., 2007).

The middle and western sites covering the main body of the Eucla Basin are less complex and can be studied with higher confidence. As a result, more conclusive study has been performed in the area and comparatively simple sedimentary sequences have been created.

Jones (1990) published a paper focussing on the sediment packages in the western region of the Eucla Basin. Drilling samples and paleontological data were used to reveal Early Cretaceous to Miocene sequences in the north-western region of the Eucla Basin.

Faulting and Structures

Among the various faults and shear zones across the Eucla Basin, one that stands out significantly is the Mundrabilla Shear Zone. Aitken et al. (2015) argue that despite the somewhat similar properties either side of this zone, structures dating back to the Mesoproterozoic are not continuous over this region. Magnetic and gravity data show the fault zone causing significant displacement which can be traced for around 3,000 km into Antarctica. The shearing is inferred to be strike-slip with sinistral sense, becoming less obvious to the north, likely due to succeeding overprinting tectonic events (Aitken et al., 2015). This shear zone stands out clearly in figure 2, noticeably displacing other features and provinces in this area.

The Karari Fault is a major normal fault zone which is north east – south west trending and lies to the east of the Eucla Basin (McLean et al., 2003). The zone is characterised by anomalously high magnetic readings expected to be sourced from the pervasive presence of mylonites. Direen et al. (2005) show that a steep, negatively trending gravity change from west to east is recorded over the Karari Fault Zone with a change of roughly 22 mGal. This change is expected to be due to the footwall of the fault zone revealing a younger basin of low density sediments.

Prospectivity

The Eucla Basin contains a unique landscape which is largely due to tectonic forces and calm climate conditions since its formation. Draining of material from these surrounding regions has led to various areas in the basin containing noteworthy mineral deposits including gold, uranium and a range of heavy minerals. A well preserved paleoshoreline sequence along the north-eastern Eucla Basin is a prospective area for

heavy mineral placer deposits.

Extensive borehole data reveal significant depositional events during the Paleocene-Early Eocene, Middle-Late Eocene, Oligocene-Early Miocene, Middle Miocene-Early Pliocene and Pliocene-Quaternary.

One potential prospective area is the western margin of the Gawler Craton. Active mining areas such as Beverly, Arkaroola, Andamooka, Olympic Dam and more exist on the eastern extent of the Gawler Craton where much of the craton is either outcropping or near to the surface. The western region of the Gawler Craton is largely covered by regolith and is therefore difficult to study compared to the eastern region. These observations suggest that the western Gawler Craton has serious prospectivity potential, but this is yet to be tested.

METHODS

The overall aim of this project is to use the interpretation MT data and other geophysical techniques to understand any geological structures and resistivity properties of the crust and upper mantle. The first step in this process is to conduct a 2 dimensional inversion of the 830 km survey from the Earth's surface down into the upper mantle. The resistivity data will then be used to produce models of the crust and upper mantle showing any significant geological structures and boundaries. These will be simple diagrams showing modelled values of resistivity along the MT transect as a function of depth. These models will be non-unique as impedance tensor will be the only data form initially studied (Stephan et al., 2015). The models will show variances in areas of conductivity which may suggest geological structures and features.

To further interpret the data, the MT will be correlated with other geophysical

techniques including gravity, magnetics and seismics. The resistivity anomalies seen using the resistivity data can be studied with these other techniques to understand what materials or structures may be the cause of these differences (Thiel, 2008). This step aims to increase the confidence of these data interpretations and reduce the non-uniqueness of any applied models. The results will be used to create a statement regarding the features and resistivity properties observed across this transect. Other areas of interest will also be noted such as the structural makeup of the Eucla Basin and the western Gawler Craton.

MT Methods

The modelling and interpretation of MT data is used to analyse the conductive properties of the Earth. Variations in Earth's electric and magnetic fields are recorded from natural sources and are used to interpret the structure of the Earth for depths ranging from the upper crust down into the mantle. The inductive field is split into two different modes, transverse electric and transverse magnetic, or TE and TM respectively. TE represents the current which flows parallel to the electric strike while TM represents the current flowing perpendicular (Simpson et al., 2005).

The depth at which investigation can be made depends on the periodicity of the MT signal. Periods measured generally lie between 10^{-3} and 10^{5} s, where the higher frequencies are used to interpret the near surface features and the lower frequencies are used for deeper investigation. The source of the MT signal comes from two different natural phenomenon, worldwide lightning activity and effects of the solar wind. Signals coming from lightning are observed at frequencies >1 Hz while the solar wind produces signals of <0.1 Hz.

A second variable in this process is the resistivity of the Earth, which has a significant effect on the depth of signal penetration. A more conductive Earth will reduce the depth of a signal, making it possible for an identical frequency to record varying depths at different locations. This process is accounted for with the Skin-Depth Formula (Equation 1) which states that the depth of signal penetration is approximated to 500, multiplied by the square root of the product of the resistivity and the signal period.

$$\delta = 500 * \sqrt{(\rho T)} \quad [1]$$

The relationship between the magnetic field and the electric field at any time is defined by an impedance tensor. When a magnetic field in a conductor induces an electric field, a delay is present between the magnetic field passing through the body and the induced electric field. This is represented by the formula shown in equation 2. 'E' is the electric field, 'H' is the magnetic field and 'Z' represents the impedance. This formula allows the value of 'Z' to be calculated from the electric and magnetic fields.

$$\begin{bmatrix} E_x \\ E_y \end{bmatrix} = \begin{bmatrix} Z_{xx} & Z_{xy} \\ Z_{yx} & Z_{yy} \end{bmatrix} \begin{bmatrix} \mathrm{H_x} \\ \mathrm{H_y} \end{bmatrix} \quad [2]$$

Once the impedance is known, it can be used to calculate the phase tensor. The phase tensor, displayed as Φ, is defined by the ratio of the real and imaginary parts of the impedance (Caldwell et al., 2004). The phase tensor formula is given in equation 3, where X^{-1} represents the inverse of the imaginary component of the impedance and Y represents the real component.

$$\Phi = X^{-1} Y \quad [3]$$

This phase tensor can be displayed graphically as an ellipse, where β is the skew angle of the major axis and the major axis is given by α – β.

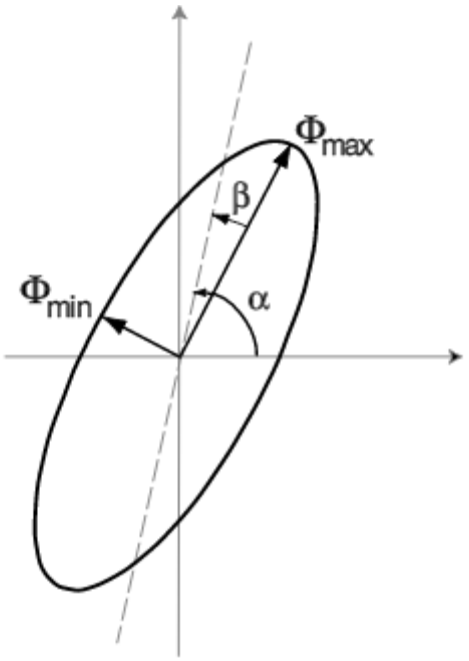

Figure 3: An illustration of the phase tensor presented as an ellipse, where the maximum and minimum Φ values are proportional to the axes of the ellipse. The angle α – β defines the direction of the major axis Φmax in relation to the reference frame. Image modified from Caldwell et al. (2004).

Once calculated, phase ellipses can be used to interpret lithological features and structures found within the Earth. The major axis of consecutive phase ellipses can be traced through pseudo-sections to show the axial strike of localised structures. Additionally, the complexity of lithologies may be determined by the ellipticity of the tensors, where the skew of the ellipses increases with data complexity.

Data Collection

The Trans-Australian railway which runs from Kalgoorlie in Western Australia to Port Augusta in South Australia provides an East-West line which crosses the Eucla Basin.

This rail line allowed the MT survey to be undertaken in a relatively straight line through a largely unexplored region of the Eucla Basin. This broadband survey was performed over an 830 km transect with a site spacing of 5 km.

RESULTS

Data

Of the 167 MT data sites, only 161 were used for modelling due to some poor quality data. The six omitted sites were all on the eastern side of the survey line where the data collected are of high complexity. For the MT modelling, a tau (τ) value of 10 was used to fit the data. This value was chosen as it appeared to smooth out the data into a simple, easy to interpret model, without discounting any important aspects of the dataset. The data errors allowed for TE were 15% for apparent resistivity and 2.5% for phase. The TM data floor errors were 5% for apparent resistivity and 2.5% for phase. The interpreted models covered a resistivity range of 10 – 10,000 Ωm. Any data points which appeared to be outliers or inaccurate due to instrument error were removed from the MT models.

Phase tensors were also calculated from the MT data across a range of frequencies. These were then plotted on both magnetic and gravity maps of the area for comparison. All phase tensors were then plotted as pseudosections for the whole of the MT line as a function of period. This was used as a means of studying resistivity structures and axial properties from the surface down into the upper mantle for every available phase tensor.

Phase Tensor Pseudosections

Pseudosections for all available phase tensors are displayed in figure 4. The major axes of the tensors display trends in strike while the ellipticity of the tensors represents the dimensionality of the data. The circular tensors show data which are 1D while elliptical tensors exist where the data are 2D or 3D. The colours of the tensors show the phase of the data at that point, where red indicates a decrease in resistivity with depth and blue indicates an increase. Major trends in strike are noted with yellow arrows while the solid yellow lines show a transition zone between phase angles higher than 45 degrees and phase angles lower than 45 degrees. Zones below this line therefore increase in resistivity with depth.

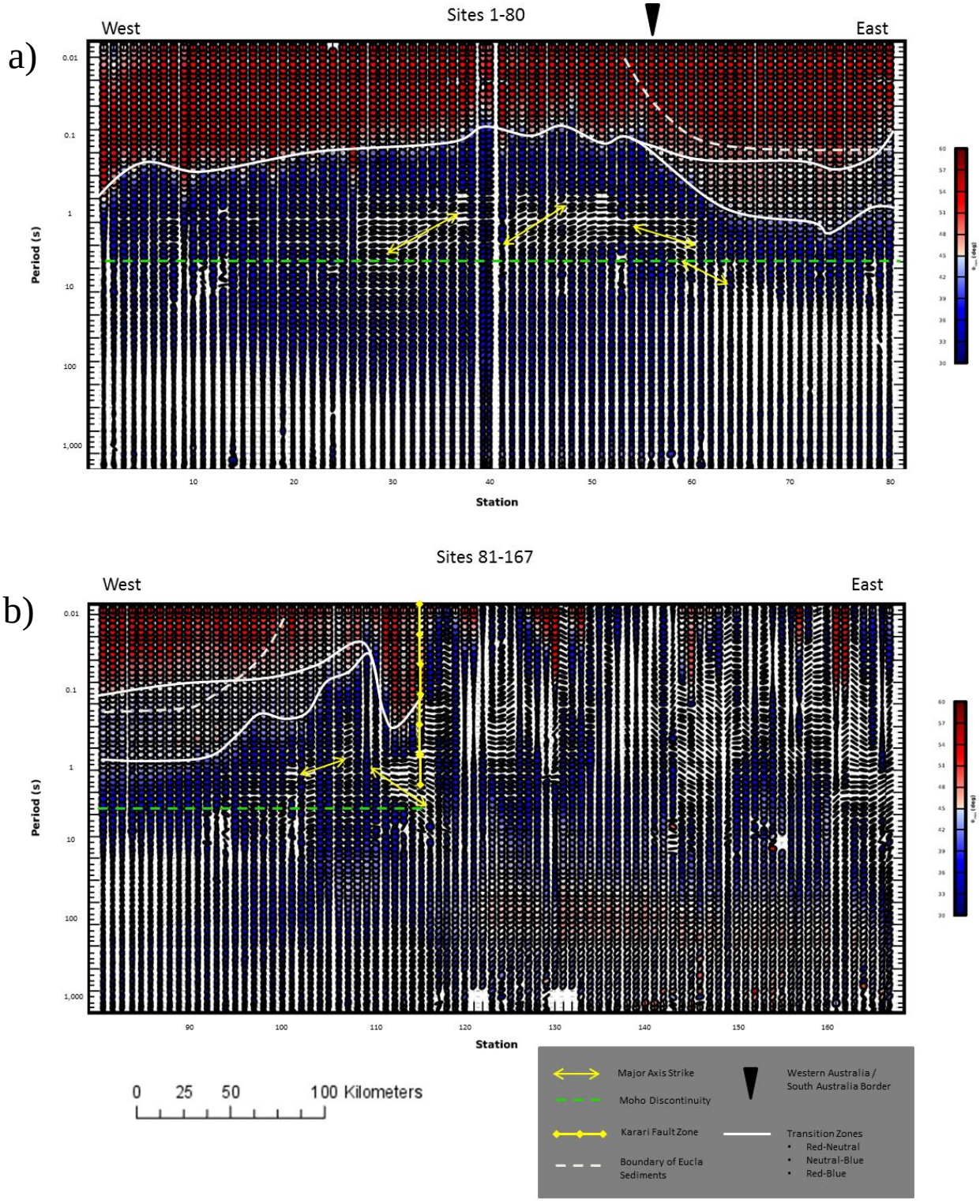

Figure 4 (a&b): Phase tensors for the western (a) and eastern (b) extent of the MT line, varying vertically with period.

Phase Tensors Plotted on Gravity and Magnetics

To compare the MT data to the regional geophysical responses in the study area, phase tensors of varying frequencies have been plotted on maps of gravity and magnetics. Due to the length of the studied transect, phase tensors were split into two lines, the west and the east. The phase tensor models interpreted were recorded at a frequency of 1Hz, as these tensors appeared to reveal the most information in the upper crust without being too complex. Figures 5 and 6 show models for the west and east sections of the line respectively. As with much of the MT data, the phase tensors become very elongated and unorientated past site 120 and consequently these sites were not used for interpretation in this part of the report.

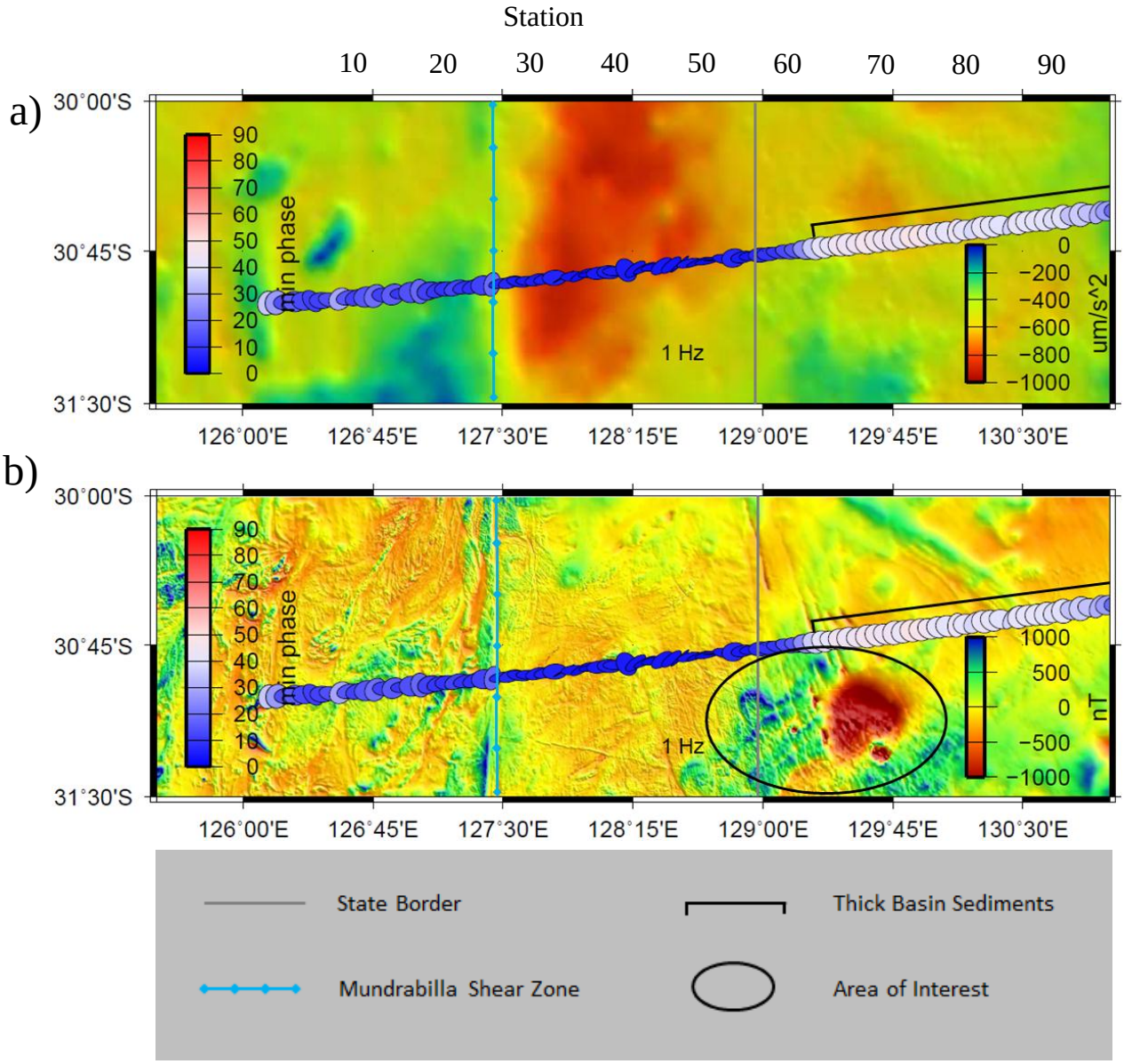

Figure 5(a&b): Phase tensors at frequencies of 1Hz for the western section of the MT transect plotted on regional gravity (a) and magnetics (b). A phase value >45 degrees indicates resistivity decreasing with depth while a phase value <45 degrees indicates resistivity increasing with depth.

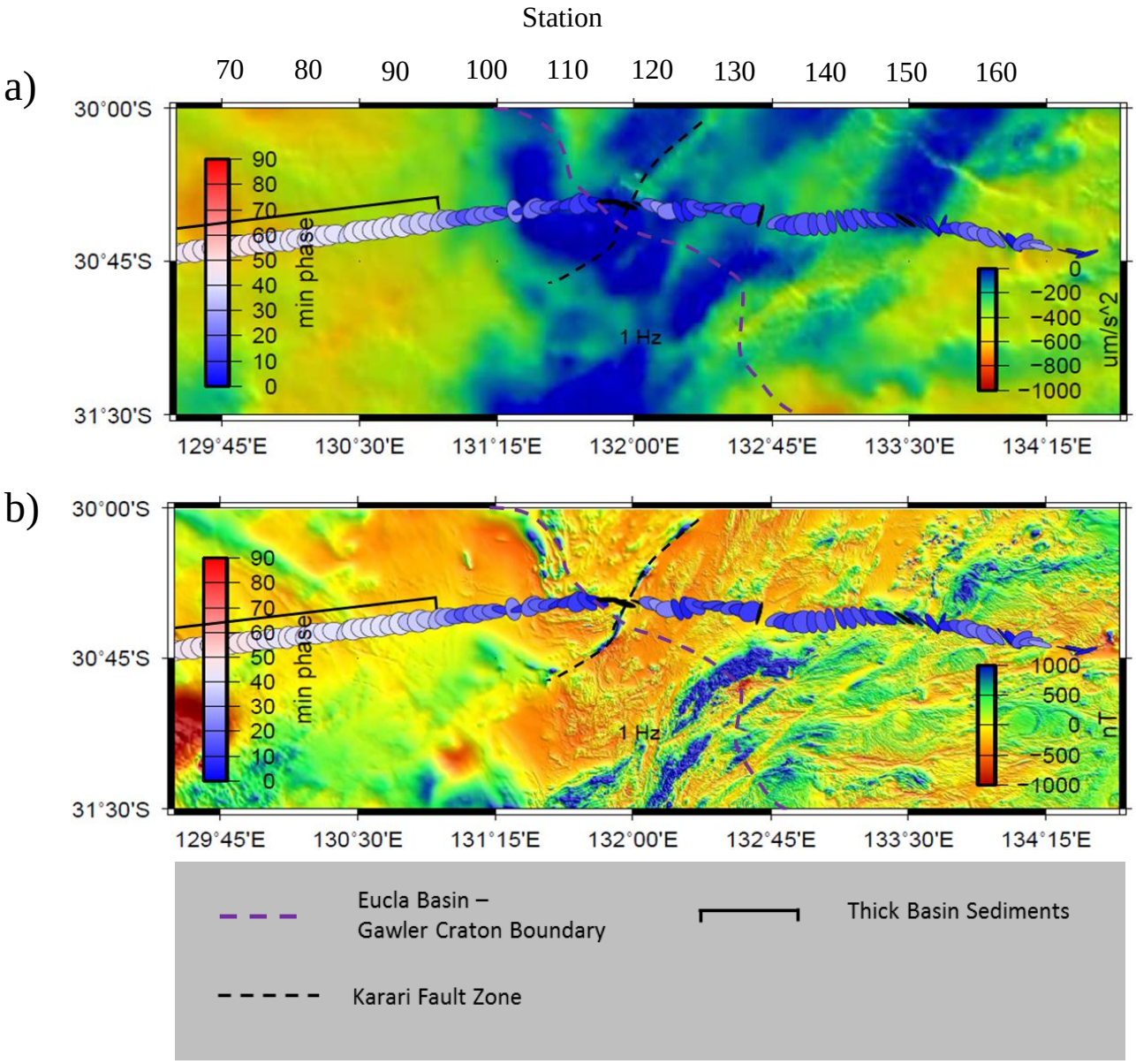

Figure 6(a&b): Phase tensors at 1Hz for the eastern section of the MT transect plotted on regional gravity (a) and magnetics (b).

2D Inversions

The type of 2D inversion used is defined by Rodi et al. (2001) as using a nonlinear conjugate gradients scheme to compute regularised solutions for 2D MT inversions. This method is shown by Rodi et al. (2001) to be the most efficient in terms of computer memory and the run time required to run inversions of realistic size.
2D MT inversions were run for all stations in the study, however the transect was too long to run a high definition inversion which would fit all sites simultaneously. Subsequently the line was split into 4 sections to cover the whole study area. Once this was completed, it was clear that significant edge effects had appeared on the models, adding and subtracting to real features existing on the margins of some inversions. To counter this, additional inversions were run over the boundaries of the previous lines, creating one continuous inversion which covered the entire MT transect with minimal edge effects. At this stage it became apparent that the data to the east of site 118 were of too high complexity to be studied with this 2D inversion. Models showing areas of interest are displayed in figures 7, 8 and 9. The Moho is plotted at a depth of roughly 40 km.

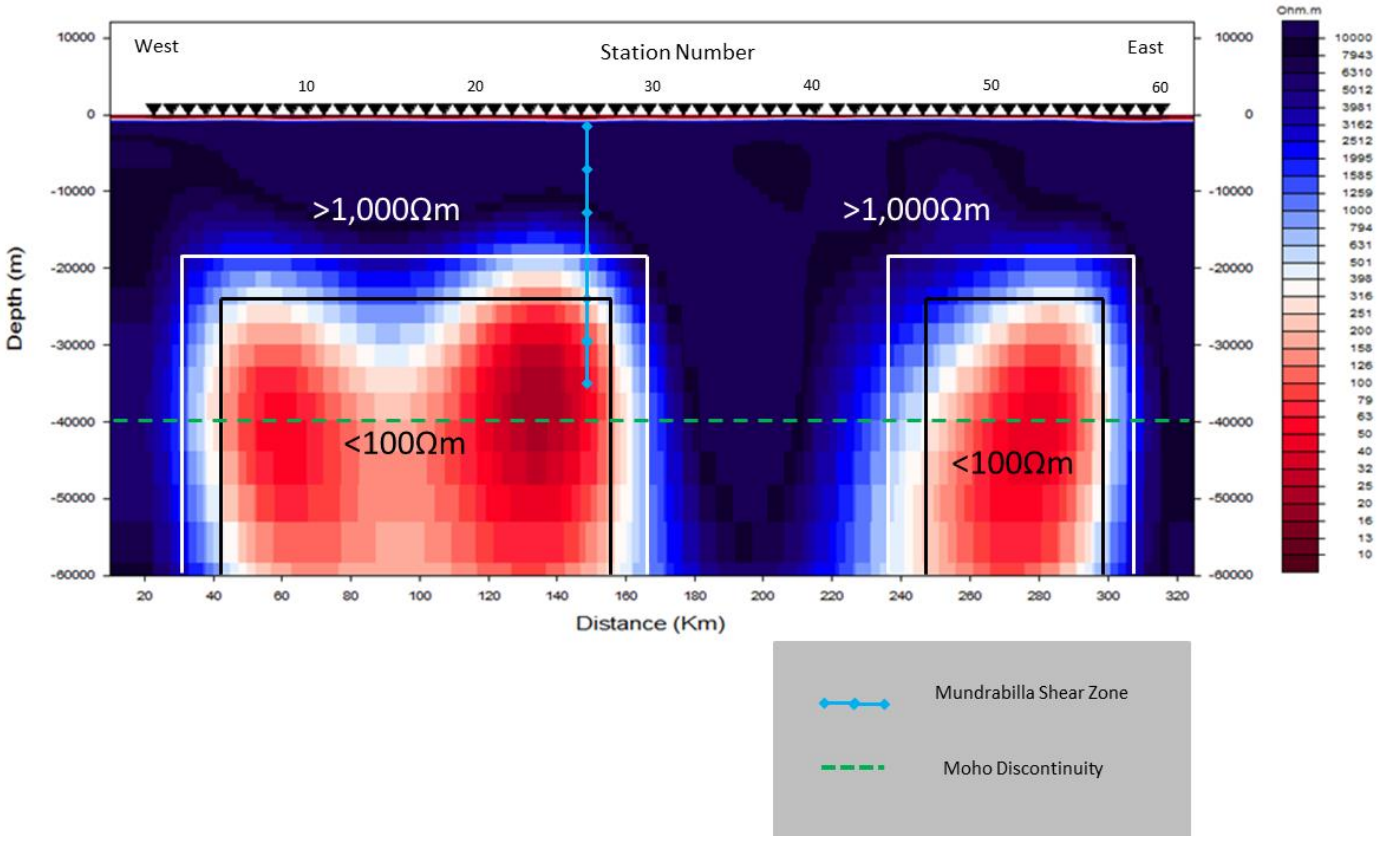

Figure 7: A 2D inversion displaying resistivity values for MT sites 1-60 at a depth of 60 km and a resistivity range of 10-10,000 Ωm. The location of the Mundrabilla Shear Zone is identified beneath site 26 and regions of notable high and low resistivities are outlined.

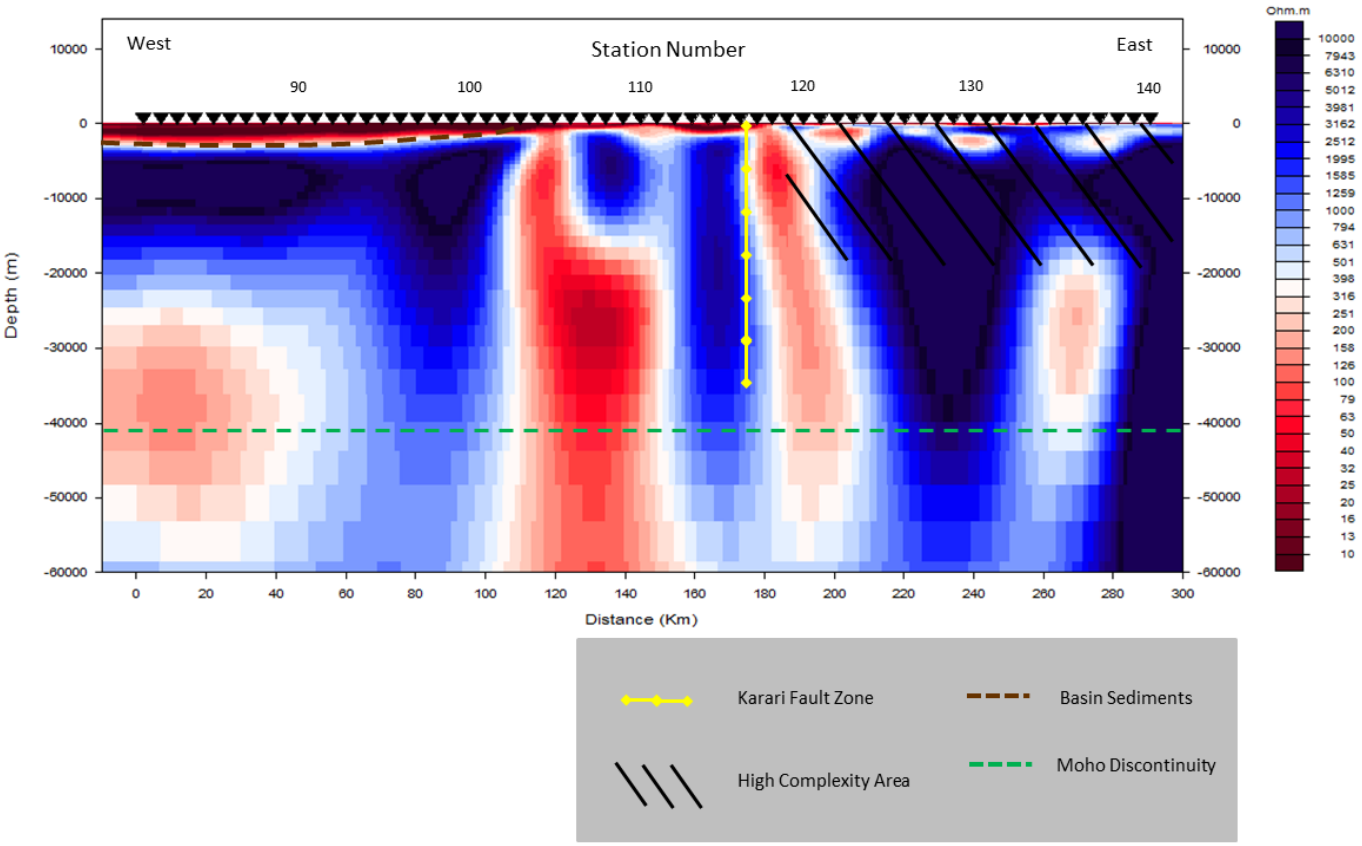

Figure 8: A 2D inversion showing resistivity levels from site 81-140 with a resistivity range of 10-10,000 Ωm used. The model is shown at a depth of 60 km and a conductive anomaly coinciding with the location of the Karari Fault Zone can be seen beneath site 115/116. Data to the east of this feature are considered too complex to confidently interpret.

A deep sedimentary package was picked up by the models between sites 60 and 100, correlating to a basin which appears to be up to 1500 m deep and roughly 200 km wide from west to east. Figure 9 shows the basin sediments changing in thickness from around 300 m in the west to around 2 km in the centre of the diagram.

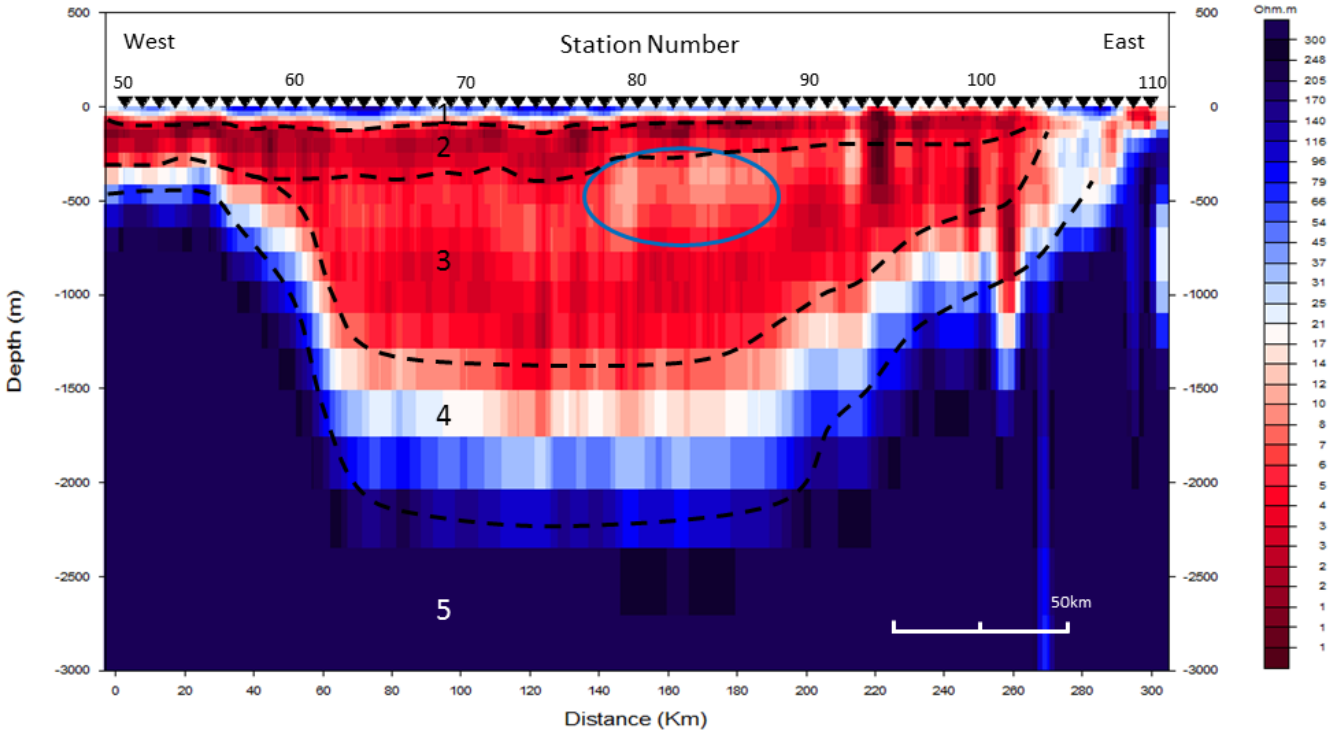

Figure 9: 2D inversion showing the thickening of the Eucla Basin sediments across sites 50-110. This model displays resistivity properties to a depth of 3 km. A resistivity range of 1-300 Ωm was used to emphasize the properties of the basin sediments. The layers are separated into 5 regions for discussion and one slightly anomalous region is circled in blue.

DISCUSSION

2D Inversions

Collected MT data are non-unique and therefore, when modelling, the same set of data can be used to produce a number of 2D inversions. To counter this, a number of models were produced to gain an understanding of which settings gave the most realistic and clear images. Other geophysical methods were also integrated with the 2D inversions to raise the confidence levels of the interpretations.

The first 2D model was completed across sites 1-60 and is displayed in figure 7. High resistivities (>1,000 Ωm) are recorded over the majority of the grid, with some zones of

enhanced lower crustal conductivity. These inconsistent features, which are seen in many areas across the transect, have an unknown origin and are likely related to the thermal and fluid evolution of the lower crust. Guo et al. (2015) say that materials likely to show highly conductive properties in the continental crust include partial melts, aqueous fluids and zones containing high densities of graphite minerals. Guo et al. (2015) came to a conclusion that high conductivity features of around 10 Ωm can often be attributed to brine-bearing albite with a fluid fraction of around 0.01. The significant gap between conductors indicates that this area of the crust can be divided into very different domains.

A sudden change in resistivity values appears to occur over the Mundrabilla Shear Zone. This fault is believed to cause a significant sinistral strike-slip offset which runs north-south for around 3,000 km (Aitken et al., 2015). This resistivity change is therefore not unexpected, as this zone is very likely to lie on the boundary of two relatively unrelated lithologies.

Figure 8 shows the inversion recorded for 80-140. The features produced by the data to the east of station 120 were deemed too unreliable to confidently interpret. Just before the data become too complex, a feature showing low resistivities (ranging roughly 50-200Ωm) coincides with the location of the Karari Fault Zone. This conductive feature is interpreted to be caused by fluids which may have travelled deep into the fault zone through fluid pathways. Any variations in resistivity throughout this zone may be due to factors including rock porosity or fluid properties such as salinity (Tsang et al., 1990).

The shallower image in figure 9 shows a representation of the resistivity properties in the basin sediments. This image shows a thin resistive layer at the surface of the basin, quickly transitioning into much more conductive material at <100 m depth and

gradually becoming more resistive around 1500 m. The basin has been defined by 5 layers represented by the dashed lines.

The first layer of resistive material (~150-200 Ωm) is interpreted to be a marine limestone, more specifically the Nullarbor Limestone which is seen throughout the area at this depth (Jones, 1990).

The shift from this material into the more conductive region, identified as layer 2, is likely to be due to the porous Eucla sediments rich in clay minerals and other conductive materials found throughout the basin (Hou et al., 2008). This layer reaches a minimum resistivity of around 1Ω m at a depth between 100 and 200 metres and abruptly shifts downward into a region of slightly higher resistivity which is seen consistently through the basin.

This pervasive area of slightly less conductive material is expected to represent the Officer Basin sediments. The Officer Basin was deposited from the Neoproterozoic to the Late Devonian and is therefore older than the Eucla Basin. The Officer Basin is in some areas overlain by the Eucla Basin, which appears to be the case in this example. The higher resistivities seen in the Officer Basin when compared to the Eucla Basin may be a consequence of lower porosity levels and therefore a higher ratio of rock to fluids. Lower porosities would be expected in the Officer Basin due to the older age of the basin and also the depth at which it exists. The difference may also be due to a composition change between basins such as a difference in clay mineral density.

The region identified as layer 4 likely represents the lower portion of the Officer Basin. The higher resistivities observed here may be a result of some mixing of sediments with basement rock, but are most likely a result of the modelling processes being unable to pick up a sudden change at this depth. Therefore it is difficult to pinpoint exactly where

the change is or declare how abruptly the basin is truncated.

Layer 5 is the final layer consisting of Precambrian gneiss and granite, making up the basement of the Eucla Basin (Jones 1990). The gradual increase in resistivity seen in some areas of the basin is attributed to changes in sediment porosity which decreases exponentially with depth (Ramm et al., 1995).

One somewhat anomalous region can be seen near the middle of the basin and is identified in figure 9 by the blue oval. This region is only slightly different in resistivity to its surrounding areas but does produce this relatively consistent reading over a significantly large area. The edges of this resistivity anomaly are plotted on figure 10.

.

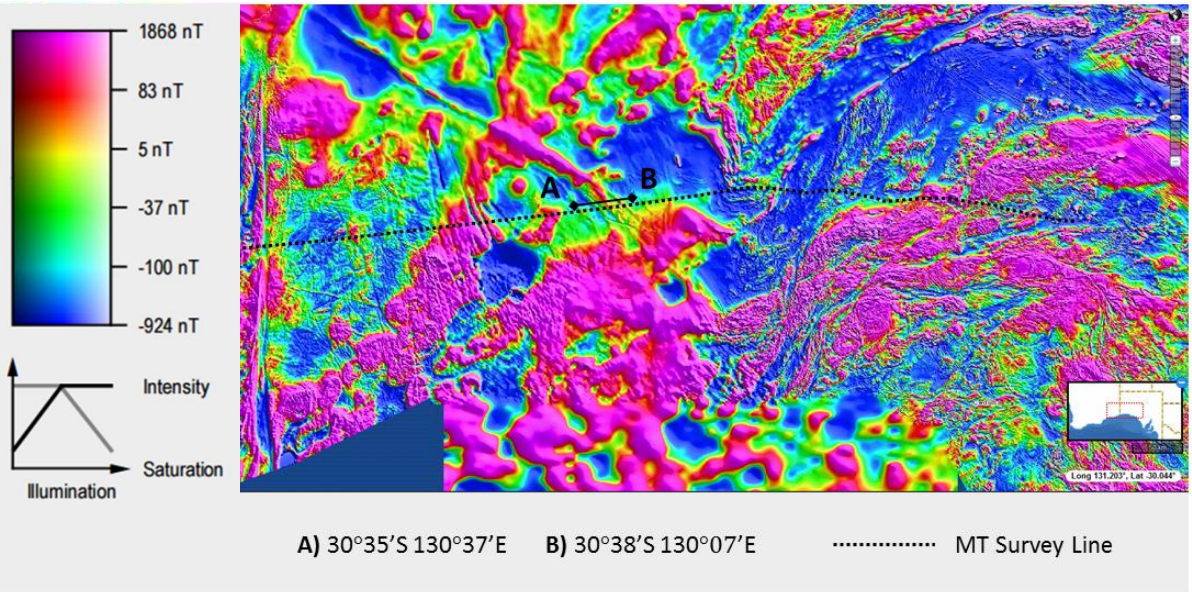

Figure 10: Map showing the MT survey line printed over a regional TMI image of the area. The line connecting points A and B shows the location of a resistivity anomaly observed in the 2D inversions. Image modified from Geoscience Australia.

As can be seen, the boundaries of this noticeable change in resistivity fall over a large dyke trending north west – south east through the area. Numerous dykes can be seen at the base of the Officer Basin and are associated with the formation of the basin in the

Neoproterozoic (Zhao et al., 1994). However, if this resistivity anomaly is representing the dyke structure seen in figure 10, it would therefore be younger in age than the basin sediments. If this is the case, this dyke is not associated with these other nearby dykes and has appeared sometime after the formation of the basin. One possibility is that this feature represents a feeder dyke to the Table Hill Volcanics which were active in the early Cambrian and caused intrusions through parts of the Officer Basin (Compston, 1974).

Phase Tensor Pseudosections

Overall, the phase tensor pseudosection figures show low apparent resistivity values for material at shorter periods (<1 second) and high values for material >10 seconds, with the transition zone generally existing between these two points. It appears that the presence of the basin sediments have altered the modelling to show low resistivities beneath the basin. The regions here appear to have more conductive properties well into the lower crust, whereas other areas are far more resistive. This result is interpreted to be a consequence of the modelling process and is therefore not discussed in depth. An axial trend in the lower crust is apparent between sites 30 and 65, with structures on the west of this trend dipping to the west and structures on the east dipping towards the east. Some structures are notable in the eastern pseudosection, although these are of lower confidence as they exist where the data become significantly more complex. Data to the east of site 120 were left uninterpreted due to a high complexity in the phase tensor properties. As can be seen in this area, the phase tensors are largely two dimensional and three dimensional and no clear trends between the tensors exist. This suggests that these examples are representing noise.

The Karari Fault Zone is found at site 115, just to the west of where the data become very difficult to interpret. No obvious phase values or axial trends appear to be affected by the fault; however due to its location, it is unclear whether this region is under the influence of noise from the complex data nearby.

Phase Tensors plotted on Magnetics and Gravity

The phase tensor data on the western extent of the survey line (See figures 5 and 6) are clearly affected by the presence of the Eucla Basin sediments. The phase tensors record low values to the west of MT site 58 coinciding with shallow sediment depth in this area. These values indicate increases in resistivity with depth likely due to conductive sediment near the surface and more resistive basement rock beneath. Where sediment load is significantly thicker to the east of site 58, phase values are close to neutral. This is anticipated as the signal used here (1 Hz) does not penetrate far into the crust and therefore would not reach the base of this sediment package, subsequently recording little to no variations in resistivity values.

Phase tensors at this frequency show a noticeable change around site 26. The sites here indicate a sudden change in axial strike and a significant increase in data complexity from west to east. This change is also picked up in both the gravity and magnetic data and is interpreted to be representing the Mundrabilla Shear Zone. The gravity data reveal a negative west to east change across this boundary.

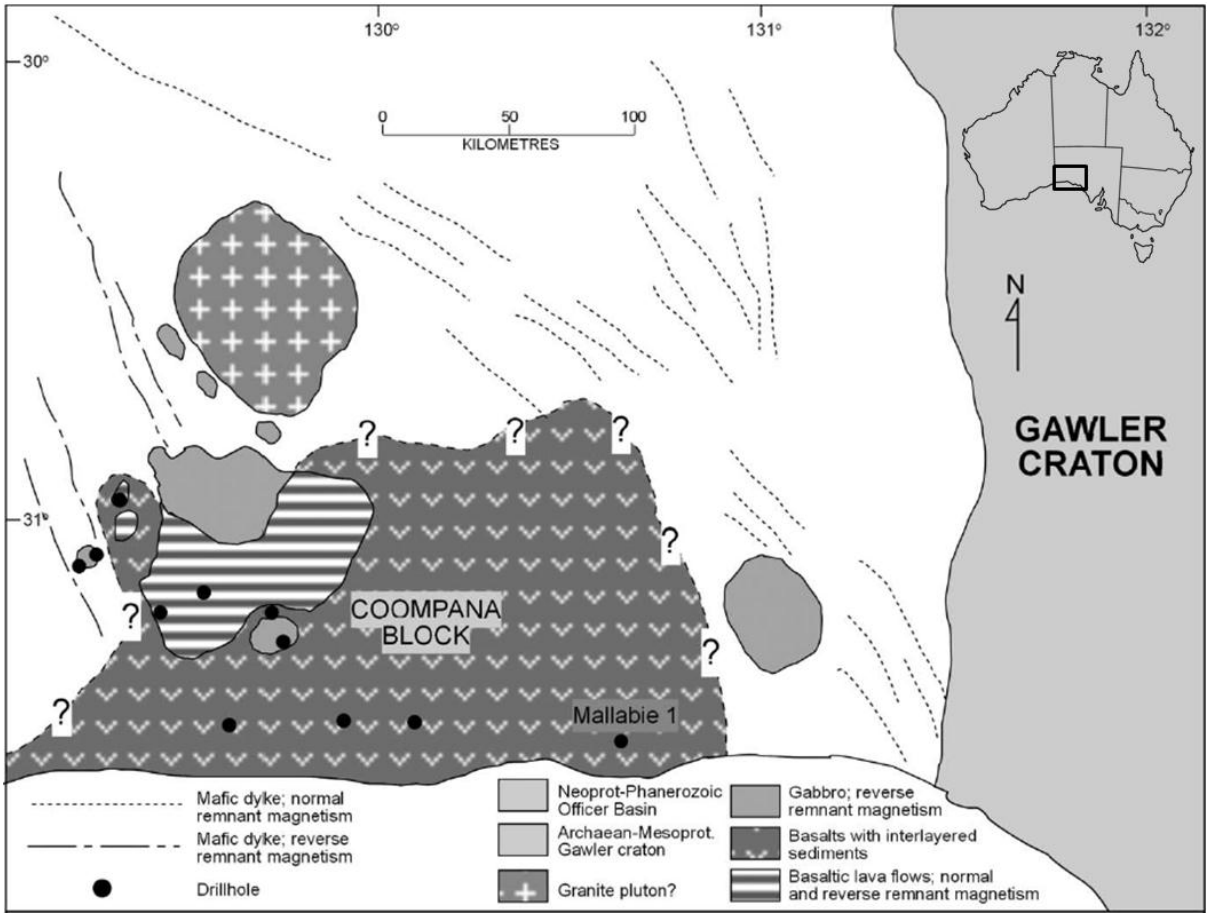

Figure 11: Map showing the geological properties and features of the Coompana Province and surrounding areas. Image modified from Wade et al. (2007).

The magnetic data reveal a series of linear structures in an area of 50 km by 50 km. These features, which are highlighted by the black oval in figure 5, exhibit low magnetic readings and trend roughly north northwest – south southeast through this region. Figure 11 shows that a number of mafic dykes, displaying demagnetised properties, exist in this area (Wade et al., 2007). The linear features found in the magnetic data are expected to represent these mafic dykes as they exhibit similar magnetic properties and are found in the same region.

Immediately to the east of here the magnetic data show a roughly circular block of anomalously low magnetic intensity. This area is picked up as a high in the gravity data

and appears to have a diameter of around 25 km. Wade et al. (2007) suggest the presence of a noticeable gabbro block in this region, appearing somewhat circular in shape and showing reverse remnant magnetism. One of these features is expected to be responsible for the gravity high and magnetic low found in the magnetic data.

A paper by Newton et al. (2003) reports the presence of various mafic intrusive plugs in the Coompana Block basement rock, which may coincide with the gabbro block picked up by Wade et al. (2007). Newton et al. (2003) also notices a system of northwest trending mafic dykes in this area. The features in figure 5 (b) are expected to correspond to these volcanic-related findings by Wade et al. (2007) and Newton et al. (2003).

The eastern extent of the study transect is much more difficult to interpret through MT phase tensors. The other geophysical data also show a noticeable increase in crustal complexity, with large scale changes in magnetic data and inconsistent readings in gravity.

A paper written by Mclean et al. (2003) identifies a number of granite intrusions less than 6km deep in the western Gawler Craton which are between 15 and 25 km in diameter. The magnetic data appear to reveal two features matching this description just south of the easternmost MT sites, providing significant evidence for their existence.

The Karari Fault Zone, running through site 115, is another feature noticeable in the regional magnetic data, showing up as a magnetic high and lying in a high gravity region. This fault zone marks a rough boundary between the more simple MT data (west) and the beginning of the high complexity features (east).

As with the western extent of the transect, the region of high sediment load to the west of site 100 records mostly neutral readings. To the east of this area, low phase values are

recorded, indicating increasing resistivity with depth. This is likely due to the relatively shallow presence of the Gawler Craton basement rock containing more resistive features than sediment lying above.

At the frequency used for this part of the investigation, the phase values appear to vary gradually across the length of the study area. As seen in the phase tensor pseudo-sections, the phase values are comparatively low (<30°) at the western extent of the line, identifying that resistivity values at these points increase with depth. This result is expected as the frequencies of these phase tensors represent relatively conductive surface sediments overlying the resistive basement material.

As the surface sediments deepen into the basin to the east of this region, the phase values trend towards neutral values (around 45°). This is a consequence of the sediment package thickening to a point where the underlying basement rock is no longer recorded by this frequency. Therefore no significant resistivity changes exist at this point and neutral phase values are produced.

Continuing to the west and coming out of the basin sediments, the phase values return to lower values as expected. The data quickly become complex around this region, however the phase values of the ellipses remain mostly constant, showing resistivity increasing downward into the basement rock.

CONCLUSIONS

The 2D inversions used to model the MT data from the Madura Province to the Gawler Craton revealed a sequence of mostly resistive (>1,000 Ωm) crust and upper mantle. Some anomalously conductive (<100 Ωm) regions were found concentrated around the Moho, though these areas produced relatively high ambiguity in the 2D inversion results. Therefore the confidence in the shape, size and location of these features was not high enough for a full interpretation. The Mundrabilla Shear Zone appears to separate two resistivity regions, while an almost vertical highly conductive feature was picked up below the Karari Fault Zone. At a depth of around 40 km, the Moho appears to cause no major resistivity changes in the MT data.

The 2D inversions were used to identify the layers in the basin sediments as the Nullarbor Limestone, the Eucla Basin and the Officer Basin. A large scale dyke was identified intruding into the Officer Basin sediments, signifying that volcanic processes were active after the deposition of the Officer Basin in the Neoproterozoic. This dyke is believed to be a result of the Table Hill Volcanics which were active during the Cambrian.

The limitations to this project include the non-uniqueness of the MT data, which lowers the confidence of applied models. Before interpretation, inversions were run at varying tau values to determine which settings gave the most realistic results. Once completed, the inversions were compared to other geophysical data before interpretation to raise confidence levels. MT data to the east of site 120 were deemed too complex to confidently interpret and subsequently the gravity and magnetic maps were the only geophysical technique used in the analysis of this area.

ACKNOWLEDGEMENTS

I would like to thank my supervisor Graham Heinson and co-supervisor Stephan Thiel for support and instruction throughout the academic year. Thanks to Paul Soeffky for computer support and help with various problems, the University of Adelaide and also Geoscience Australia and the Geological Surveys of WA and SA for supplying the MT data.
Thanks also to the honours supervisor Katie Howard for continued guidance and Rian Dutch from the Geological Survey of South Australia, for valuable information and suggestions for my thesis.

REFERENCES

Aitken A. R. A., Betts P. G., Young D. A., Blankenship D. D., Roberts J. L. & Siegert M. J. The Australo-Antarctic Columbia to Gondwana transition, *Gondwana Research*.

Benbow M. C. 1990 Tertiary coastal dunes of the Eucla Basin, Australia, *Geomorphology* 3, 9-29.

Betts P., Giles D., Lister G. & Frick L. 2002 Evolution of the Australian lithosphere, *Australian Journal of Earth Sciences* 49, 661-695.

Caldwell T. G., Bibby H. M. & Brown C. 2004 The magnetotelluric phase tensor, *Geophysical Journal International* 158, 457-469.

Clarke J. D. A., Gammon P. R., Hou B. & Gallagher S. J. 2003 Middle to Upper Eocene stratigraphic nomenclature and deposition in the Eucla Basin, *Australian Journal of Earth Sciences* 50, 231-248.

Compston W. 1974 The table hill volcanics of the officer Basin—Precambrian or Palaeozoic?, *Journal of the Geological Society of Australia* 21, 403-411.

Feary D. A. & James N. P. 1995 Cenozoic biogenic mounds and buried Miocene(?) barrier reef on a predominantly cool-water carbonate continental margin—Eucla basin, western Great Australian Bight, *Geology* 23, 427-430.

Guo X., Yoshino T. & Shimojuku A. 2015 Electrical conductivity of albite–(quartz)–water and albite–water–NaCl systems and its implication to the high conductivity anomalies in the continental crust, *Earth and Planetary Science Letters* 412, 1-9.

Hand M., Reid A. & Jagodzinski L. 2007 Tectonic framework and evolution of the Gawler Craton, southern Australia, *Economic Geology* 102, 1377-1395.Hou B., Alley N. F., Frakes L. A., Stoian L. & Cowley W. M. 2006 Eocene stratigraphic succession in the Eucla Basin of South Australia and correlation to major regional sea-level events, *Sedimentary Geology* 183, 297-319.

Hou B., Frakes L. A., Sandiford M., Worrall L., Keeling J. & Alley N. F. 2008 Cenozoic Eucla Basin and associated palaeovalleys, southern Australia — Climatic and tectonic influences on landscape evolution, sedimentation and heavy mineral accumulation, *Sedimentary Geology* 203, 112-130.

Hou B., Alley N. F., Frakes L. A., Stoian L. & Cowley W. M. 2006 Eocene stratigraphic succession in the Eucla Basin of South Australia and correlation to major regional sea-level events, *Sedimentary Geology* 183, 297-319.

Howard K. E., Hand M., Barovich K. M., Payne J. L. & Belousova E. A. 2011 U–Pb, Lu–Hf and Sm–Nd isotopic constraints on provenance and depositional timing of metasedimentary rocks in the western Gawler Craton: Implications for Proterozoic reconstruction models, *Precambrian Research* 184, 43-62.

Jones B. G. 1990 Cretaceous and Tertiary sedimentation on the western margin of the Eucla Basin, *Australian Journal of Earth Sciences* 37, 317-329.

Li Q., James N. P., Bone Y. & McGowran B. 1996 Foraminiferal biostratigraphy and depositional environments of the mid-Cenozoic Abrakurrie Limestone, Eucla Basin, southern Australia, *Australian Journal of Earth Sciences* 43, 437-450.

McGowran B. 1989 The later Eocene transgressions in southern Australia, *Alcheringa: An Australasian Journal of Palaeontology* 13, 45-68.

McLean M. A. & Betts P. G. 2003 Geophysical constraints of shear zones and geometry of the Hiltaba Suite granites in the western Gawler Craton, Australia, *Australian Journal of Earth Sciences* 50, 525-541.

Newton W., Daly S., Burtt A., Priess W., Conor C. & Robertson S. 2003 Overview of geology and mineralisation in South Australia, *ASEG Extended Abstracts* 2003, 1-17.

Ramm M. & Bjorlykke K. 1994 Porosity/depth trends in reservoir sandstones; assessing the quantitative effects of varying pore-pressure, temperature history and mineralogy, Norwegian Shelf data, *Clay Minerals* 29, 475-490.

Rodi W. & Mackie R. L. 2001 Nonlinear conjugate gradients algorithm for 2-D magnetotelluric inversion, *Geophysics* 66, 174-187.

Simpson F. & Bahr K. 2005 Practical Magnetotellurics. Cambridge University Press.

Spaggiari C. V., Kirkland C. L., Smithies R. H., Wingate M. T. D. & Belousova E. A. 2015 Transformation of an Archean craton margin during Proterozoic basin formation and magmatism: The Albany–Fraser Orogen, Western Australia, *Precambrian Research* 266, 440-466.

Stepan M., Heinson G., Taylor D., Robertson K., Skladzien P. & Boren G. 2015 Magnetotelluric imaging of a Palaeozoic Andean margin subduction zone in western Victoria, *ASEG Extended Abstracts* 2015, 1-2.

Thiel S. 2008 Modelling and inversion of magnetotelluric data for 2-D and 3-D lithospheric structure, with application to obducted and subducted terranes. University of Adelaide.

Thiel S. & Heinson G. 2010 Crustal imaging of a mobile belt using magnetotellurics: An example of the Fowler Domain in South Australia, *Journal of Geophysical Research: Solid Earth* 115, n/a-n/a.

Tsang C.-F., Hufschmied P. & Hale F. V. 1990 Determination of fracture inflow parameters with a borehole fluid conductivity logging method, *Water Resources Research* 26, 561-578.

Wade B. P., Payne J. L., Hand M. & Barovich K. M. 2007 Petrogenesis of ca 1.50 Ga granitic gneiss of the Coompana Block: filling the 'magmatic gap' of Mesoproterozoic Australia, *Australian Journal of Earth Sciences* 54, 1089-1102.